Chemical induction of unfolded protein response enhances cancer cell killing through lytic virus infection

Prasad, Vibhu ; Suomalainen, Maarit ; Pennauer, Mirjam ; Yakimovich, Artur ; Andriasyan, Vardan ; Hemmi, Silvio ; Greber, Urs F

Abstract: Cancer cells are susceptible to oncolytic viruses, albeit variably. Human adenoviruses (HAdVs) are widely used oncolytic agents, engineered to produce progeny within the tumor, and elicit bystander effects. We searched for host factors enhancing bystander effects, and conducted a targeted RNA-interference screen against guanine-nucleotide exchange factors (GEFs) of small GTPases. We show that unfolded protein response (UPR), which is readily inducible in aggressive tumor cells, enhances melanoma or epithelial cancer cell killing upon HAdV infection. UPR was triggered by knock-down of Golgi Brefeldin-A resistant guanine-nucleotide-exchange factor-1 (GBF-1), or the GBF-1 inhibitor Golgicide A (GCA), and stimulated HAdV infection. GBF-1 is a GEF for ADP-ribosylation factors (Arfs) regulating ER to Golgi and intra-Golgi transport. Cells treated with GCA enhanced HAdV-induced cytopathic effects in epithelial and melanoma cancer but not normal cells, if the drug was applied several hours prior to HAdV inoculation. This was shown by real-time label-free impedance measurements using xCELLigence™. GCA-treated cells contained fewer incoming HAdV than control cells, but boosted HAdV titers and spreading in cancer cells. GCA enhanced viral gene expression, or transgene expression from the cytomegalovirus promoter of B- or C-species HAdVs, but did not enhance viral E1A expression in uninfected cell lines, or cells transfected with plasmid reporter DNA. The UPR-enhanced cell killing required the nuclease activity of the UPR-sensor inositol-requiring enzyme 1 (IRE-1), and X-box binding protein 1 (XBP-1), which alleviate ER stress. The collective results show that chemical UPR induction and viruses boost tumor cell killing by enhancing oncolytic viral efficacy. IMPORTANCE Cancer is difficult to combat. A wide range of oncolytic viruses show promise for killing cancer cells. Yet, the efficacy of oncolytic killing is low. We searched for host factors enhancing adenovirus cancer cell killing, and found that the knock-down of GBF-1 (Golgi Brefeldin-A resistant guanine-nucleotide-exchange factor-1) or chemical inhibition of GBF-1 enhanced adenovirus infection by triggering the IRE- 1/XBP-1 branch of the unfolded protein response (UPR). IRE-1/XBP-1 promote cell survival, and enhanced the levels of the adenoviral immediate early gene product E1A, virus spreading, and killing of cancer cells. Aggressive tumor cells depend on a readily inducible UPR, and hence present prime targets for a combined strategy involving adenoviruses and small chemicals inducing UPR.

DOI: https://doi.org/10.1128/JVI.02156-14

Prasad, Vibhu; Suomalainen, Maarit; Pennauer, Mirjam; Yakimovich, Artur; Andriasyan, Vardan; Hemmi, Silvio; Greber, Urs F (2014). Chemical induction of unfolded protein response enhances cancer cell killing through lytic virus infection. Journal of Virology, 88(22):13086-13098.
DOI: https://doi.org/10.1128/JVI.02156-14

Chemical Induction of Unfolded Protein Response Enhances Cancer Cell Killing through Lytic Virus Infection

Vibhu Prasad [1, 2], Maarit Suomalainen[1], Mirjam Pennauer[1], Artur Yakimovich[1], Vardan Andriasyan [1, 2], Silvio Hemmi[1], Urs F. Greber[1, 3]

[1] Institute of Molecular Life Sciences, University of Zurich, Zurich, Switzerland

[2] Molecular Life Sciences Graduate School, ETH and University of Zurich, Switzerland

[3] corresponding author: E-mail: urs.greber@imls.uzh.ch, Telephone: +41 44 635 48 41, Fax: +41 44 635 68 17

Keywords:
adenovirus / rhinovirus / cytopathic effect / melanoma cancer / Unfolded Protein Response UPR / lytic infection / oncolytics / impedance / IRE-1 / XBP-1 / gene expression / early and late genes / transcription factor

Running Title:
UPR enhances virus infection and cancer cell killing

ABSTRACT

Cancer cells are susceptible to oncolytic viruses, albeit variably. Human adenoviruses (HAdVs) are widely used oncolytic agents, engineered to produce progeny within the tumor, and elicit bystander effects. We searched for host factors enhancing bystander effects, and conducted a targeted RNA-interference screen against guanine-nucleotide exchange factors (GEFs) of small GTPases. We show that unfolded protein response (UPR), which is readily inducible in aggressive tumor cells, enhances melanoma or epithelial cancer cell killing upon HAdV infection. UPR was triggered by knock-down of Golgi Brefeldin-A resistant guanine-nucleotide-exchange factor-1 (GBF-1), or the GBF-1 inhibitor Golgicide A (GCA), and stimulated HAdV infection. GBF-1 is a GEF for ADP-ribosylation factors (Arfs) regulating ER to Golgi and intra-Golgi transport. Cells treated with GCA enhanced HAdV-induced cytopathic effects in epithelial and melanoma cancer but not normal cells, if the drug was applied several hours prior to HAdV inoculation. This was shown by real-time label-free impedance measurements using xCELLigence™. GCA-treated cells contained fewer incoming HAdV than control cells, but boosted HAdV titers and spreading in cancer cells. GCA enhanced viral gene expression, or transgene expression from the cytomegalovirus promoter of B- or C-species HAdVs, but did not enhance viral E1A expression in uninfected cell lines, or cells transfected with plasmid reporter DNA. The UPR-enhanced cell killing required the nuclease activity of the UPR-sensor inositol-requiring enzyme 1 (IRE-1), and X-box binding protein 1 (XBP-1), which alleviate ER stress. The collective results show that chemical UPR induction and viruses boost tumor cell killing by enhancing oncolytic viral efficacy.

IMPORTANCE

Cancer is difficult to combat. A wide range of oncolytic viruses show promise for killing cancer cells. Yet, the efficacy of oncolytic killing is low. We searched for host factors enhancing adenovirus cancer cell killing, and found that the knock-down of GBF-1 (Golgi Brefeldin-A resistant guanine-nucleotide-exchange factor-1) or chemical inhibition of GBF-1 enhanced adenovirus infection by triggering the IRE-1/XBP-1 branch of the unfolded protein response (UPR). IRE-1/XBP-1 promote cell survival, and enhanced the levels of the adenoviral immediate early gene product E1A, virus spreading, and killing of cancer cells. Aggressive tumor cells depend on a readily inducible UPR, and hence present prime targets for a combined strategy involving adenoviruses and small chemicals inducing UPR.

INTRODUCTION

Cancer is a devastating multifactorial disease, and difficult to combat owing to genomic instability, uncontrolled proliferation, dissemination, and poor immunologic control (for reviews, see 8, 25). Oncolytic viruses are an emerging therapeutic practice (reviewed in 1, 53). Oncolytic viral therapy takes advantage of the fact that many enveloped and non-enveloped viruses destroy host cells as parts of their replication strategy. Oncolytic viruses include herpes virus, measles virus, vesicular stomatitis virus, influenza A virus, Newcastle disease virus, vaccinia virus, poliovirus, parvovirus and adenovirus. Currently, human adenoviruses (HAdVs) are the most widely used oncolytic agents, engineered to produce progeny within the tumor, and kill tumor rather than normal cells (20).

Oncolytic viruses directly kill cancer cells, and may trigger an immune response against cancer specific or viral epitopes presented on major histocompatibility class 1 protein to immune cells. This poses the problem that an oncolytic virus can be eliminated by the immune system before reaching full efficacy, for example, if the host is not tolerant against immune-dominant viral antigens. Since immune-tolerance against dominant viral antigens is rare, other ways are explored to enhance the oncolytic efficacy of viruses. For example, treatments with biological agents, chemicals or physical induction of stress sensitize tumor cells to be killed by oncolytic viruses (3, 67). In some instances, stress induction leads to inhibition of virus replication, for example radiation therapy attenuates vaccinia virus infection (35). Alternatively, inhibition of cell stress can enhance oncolysis, for example blockage of ER stress augments rhabdovirus oncolysis (40).

Here, we report that chemical or genetic inhibition of GBF-1 (Golgi Brefeldin-A resistant guanine-nucleotide-exchange factor-1) activates unfolded protein response (UPR) from the ER, and enhances gene expression from adenoviruses HAdV-C5 and B3. GBF-1 inhibition boosts HAdV-induced cell killing, and viral dissemination in human lung epithelial or melanoma-derived cancer cells. GBF-1 is a cis-Golgi guanine nucleotide exchange factor (GEF) for ADP ribosylation factors (ARFs), and regulates ER-Golgi and intra-Golgi membrane traffic (12, 74). It is widely expressed in human cells, and controls the dynamics of ARF and COP-I at ER-Golgi interface (41, 63). Notably, GBF-1 depletion by RNAi induces the UPR by locating site specific protease (SP) 1 and 2 from Golgi to ER, and proteolytic activation of activating transcription factor 6 (ATF-6) (11).

HAdVs are wide-spread non-enveloped DNA viruses causing mild, self-limiting infections in immune-competent individuals (21). Species B and C HAdVs target the urogenital and respiratory tracts, and have been extensively developed into vectors for clinical therapy (20). They attach to host cells via the coxsackievirus adenovirus receptor (CAR), CD46 or desmoglein-2 and in most cases integrin secondary receptors (71). This triggers initial steps of virus uncoating, internalization and endosomal membrane rupture by pH-independent mechanisms (5, 46, 61). Cytosolic viruses are transported by dynein/dynactin and microtubules to the nuclear pore complex, where kinesin-mediated virus disassembly and disruption of the nuclear pore complex occur, and viral DNA is imported into the nucleus (4, 60, 62, 70). Expression of the early region 1A (E1A) genes from episomal viral DNA controls a range of host and viral genes (14, 48). E1A starts the viral gene expression and genome replication programs, which drive viral immune escape and, ultimately, the release of progeny viruses from the nucleus upon cell lysis (66). Yet, the clinical oncolytic efficacy of adenoviruses and other virus-derived oncolytic vectors has been modest (44, 65). This is paralleled by a recent observation from 2-dimensional cell cultures showing that inefficient viral transmission correlates with low events of lytic infection (72). The results here show that induction of UPR through the IRE-1 sensor and the XBP-1 transcription factor leads to enhanced viral cytotoxicity in primary human cancer cells. This is a hereto unknown pathway leading from ER stress and host transcriptional response to enhanced viral gene expression and oncolysis.

MATERIALS AND METHODS

Cells and viruses

Cells and viruses were grown as described before (5, 19, 39, 47). A549 cells (American Type Culture Collection) are human lung epithelial carcinoma cells, HeLa-ATCC is a HeLa clone obtained from American Type Culture Collection, 911 cells are human embryonic retinoblasts containing the base pairs 79-5789 of HAdV-C5 genome (16), 293T cells are human embryonic kidney cells containing the base pairs 1-4344 of HAdV-C5 genome (15, 38), and WI38 is a human diploid cell line

derived from normal embryonic lung tissue (American Type Culture Collection). XBP-1 -/- and wildtype control mouse embryonal fibroblasts (MEFs, obtained from Laurie Glimcher, Weill Cornell Medical College) were maintained as described (36). The replicating HAdV-C5_wt and HAdV-C2-dE3B_GFP were grown in A549 cells as described (22, 23, 47). Non-replicating HAdV-C5-dE1_GFP (19, 47) and HAdV-B3-dE1_GFP (57) containing GFP under the control of the CMV major immediate early promoter were grown in 911 cells. The formation of HAdV-C2-dE3B_GFP progeny was as described (49, 72). Cell viability was measured by resazurin as described (33). Infectious titer of HAdV-C5_wt and HAdV-C2-dE3B_GFP was determined on A549 cells, and that of HAdV-C5-dE1_GFP on 911 cells.

Transfections and infections

Knockdown experiments were performed in 96-well imaging plates (Greiner Bio-one) using reverse transfection: siRNA (1 pmol/well diluted in 5 µl ddH_2O, Dharmacon Smart Pool: ON-TARGET Plus) or siPools (siTools Biotech GmbH, Martinsried, Germany, 26) were mixed with Lipofectamine RNAiMAX (0.2 µl/well, Invitrogen) in 19.8 µl Optimem (Invitrogen), incubated at room temperature for 5 min, and 6,000 A549 cells/well were added in 75 µl of growth medium. The medium was changed next day to fresh growth medium and 48h post transfection, cells were infected with HAdV-C5_wt [multiplicity of infection (MOI) 0.09] or HAdV-C5-dE1_GFP (MOI 0.07) for 18 h, fixed and stained with 4′,6-diamidin-2-phenylindol (DAPI), or, in the case of HAdV-C5-wt infection, immunostained with rabbit anti-protein VI antibody (5) and secondary AlexaFluor488-conjugated anti-rabbit antibody (Life Technologies). DAPI stain was used to mark the cell nucleus, and a custom made script (Matlab, Mathworks, USA) or a custom made CellProfiler 2.0 pipeline (according to 7) were used to quantify the average nuclear intensity of the GFP and protein VI signals, which were used as measures of infection efficiency. The spreading of HAdV-C2-dE3B_GFP was analyzed by time lapse fluorescence microscopy as described (72). A detailed description of the imaging procedures is available on request. Human rhinovirus species A type A1 (HRV-A1A) infections were analyzed 7 h pi as described (34).

In Golgicide A (GCA, Sigma) experiments, the cells were pretreated with the drug or its solvent DMSO for 5 h. GCA concentration in all experiments was 20 µM. To determine virus progeny formation from control vs GCA-treated cells, HAdV-C2-dE3B_GFP (0.008 infectious units/cell) was added to confluent A549 cells and

progeny collected from the clarified culture medium, and from cells by Freon extraction 40 h post infection (pi). Samples were titrated on HeLa-ATCC cells grown on 96-well imaging plates using serial 10-fold dilutions of cell extracts or culture supernatants, at 18 h post infection samples were fixed, DAPI-stained and GFP positive cells were counted from wells that had lower than 100% infection. One GFP positive cell was scored as one infectious particle.

Cell impedance measurements by xCELLigence™ and cell counting

The xCELLigence™ system (Roche Applied Science and ACEA Biosciences) consists of four components, analyzer, device station, control unit with software and E-plates (disposable E-Plate 16). The device was used as described by the supplier (59). E-plates have a gold plated sensor array at the bottom, which measures electrical impedance across the plate. Impedance is recorded in terms of a dimensionless quantity termed cell index (CI). For background measurements, 100 µl of culture medium was added to the E-plate well, equilibrated at 37˚C and supplemented with 6,500 or 25,000 cells at 37˚C. Forty-eight hours later, inhibitor was added to the cells for 5 h, followed by the addition of virus. Impedance was recorded every 15 minutes until the CI value reached background levels. Regression analyses and graphs were rendered in GraphPad Prism (GraphPad Software Inc.). To quantify the cytopathogenicity of HAdV infection, CI values were plotted against time and ΔCIT_{50}, i.e. the time point when the CI of infected cells had decreased to 50% of maximum CI of non-infected cells, was determined.

Differential interference contrast (DIC) images of A549 cells seeded on 96-well optical plates were obtained with a bright field microscope equipped with an AxioCam MRc5 camera (Carl Zeiss). For segmentation, images were enhanced using the band-pass filter and contrast enhanced in Image J. Manual counting of cells was performed using Image J built-in plugin cell counter.

Immunoblot assays

A549 cells grown in a 24-well plate were infected with HAdV-C5_wt (2 µg / sample) at 37˚C for 5 or 9 h, cell extracts prepared in hot SDS-PAGE sample buffer, boiled,

sheared through a 20-G needle and analyzed on 15% polyacrylamide gel. Proteins were transferred to PVDF membrane by semi-dry blotting (Hoefer TE 77, Amersham Biosciences). The membrane was blocked in 5% milk powder and incubated with M73 anti-E1A (Millipore, #05-599), anti-GBF-1 (BD Biosciences, #612116), anti-IRE-1 (Cell Signaling Technology, #3294), anti-XBP-1 (Santa Cruz, #7160), anti-protein VI (5) or anti-β-tubulin antibodies (Amersham), washed with Tris-buffered saline with 0.1% Tween 20 and incubated with horseradish peroxidase (HRP)-coupled secondary antibody (Cell Signaling Technology) followed by chemi-luminescence development using Amersham Hyperfilm ECL kit (GE Healthcare).

XBP-1 splicing

cDNA was synthesized from total RNA extracts and RT-PCR carried out with primers spanning XBP-1 as described (42). PCR products were restriction digested with PstI and analyzed by 2% agarose gel electrophoresis.

GCA effects on gene expression from transfected or integrated DNA

293T cells were treated with GCA for 5 h, and E1A levels were scored from cell extracts by immunoblotting with M73 anti-E1A antibody. pMAX-EGFP plasmid DNA (Amaxa) driving GFP expression from the CMV promoter was transfected into A549 cells using Neon transfection (Life Technologies). After 24 h, transfected cells were treated with GCA for 5 h, washed, stained with Hoechst 33342, live imaged by automated high-throughput microscopy 5 or 21 h after drug washout, and single cells were analyzed for GFP expression by CellProfiler using a nuclear DAPI mask extended by 5-pixels to account for cytoplasmic GFP.

Effect of GCA on HAdV-C5 binding to cells

Cells grown on Alcian blue-coated coverslips were treated with GCA (20 μM) for 12 or 0.5 h followed by inoculation with atto 565-labelled HAdV-C5_wt at cold for 30 min, washing and 5 min pulse at 37°C. Confocal maximal intensity projections were analyzed with a custom made Matlab™ script, in which the cell outline was manually

segmented using boosted DAPI channel. The number of virus particles per cell was counted within the cell outlines and analyzed using Graphpad Prism, and Mann-Whitney test for statistics.

Statistical analyses

Results for infection assays are shown as means from 3 parallel wells, unless otherwise indicated and experiments were repeated 3 to 4 times.

RESULTS

Inhibition of GBF-1 enhances post entry steps in HAdV infection

In search for host factors enhancing bystander effects and cell killing upon viral infection, we conducted an RNA-interference screen against guanine-nucleotide exchange factors (GEFs) of small GTPases implicated in secretion. The knock-down of GBF-1 stimulated adenovirus infection, measured with HAdV-C5 wild type (wt), replication-defective HAdV-C5-dE1_GFP and replication-competent HAdV-C2-dE3B_GFP (Fig. 1 A). In both HAdV-C5-dE1_GFP and HAdV-C2-dE3B_GFP, GFP was under the major early cytomegalovirus (CMV) promoter. The extent of infection boost was between threefold and tenfold in different independent experiments and the boost with different GBF-1 siRNAs correlated with GBF-1 knockdown (Fig. 1 B-D).

We next employed a specific inhibitor of GBF-1, Golgicide A (GCA). GCA stabilizes GBF-1 on ER-Golgi membranes and interferes with ER-Golgi and intra-Golgi transport, and disperses the Golgi (54). Twenty μM GCA dispersed Golgi in A549 cells, but had no strong effects on metabolic cell activity, shown by immunostaining of giantin and resazurin measurements, respectively (Fig. 2 A, B). GCA treatment of A549 cells for at least 5 h prior to infection enhanced infection with replicating and non-replicating HAdV-B and C, as measured by GFP transgene expression, but did not affect CMV-promoter driven GFP expression from transfected plasmid DNA (Fig. 2 C, D, E). This suggested that the enhancement was not merely due to a promoter effect. The enhancement was also not due to increased virus association with cells, since quantification of atto565-labeled HAdV-C5 virus on A549 cells after 30 min virus binding at cold and 5min warm-up at 37°C indicated a less efficient virus binding to GCA-treated cells than to control cells (Fig. 2 F). If GCA was added shortly before or after virus, essentially no boosting effect was observed, strongly suggesting that GBF-1 is not acutely involved in infection, but rather through a mechanism that takes hours to build up (Fig 2 G). In further experiments we used a 5 h GCA pretreatment to induce the infection enhancing effect.

Fig. 3 shows the effect of GCA on HAdV-C viral gene expression and progeny formation. E1A, the first viral gene expressed after delivery of the HAdV genome into the nucleus, produces five different mRNAs through differential splicing. The abundance of these transcripts is temporally regulated with the largest two transcripts (13S and 12S) dominating early in infection, and the smallest (9S) being more abundant late in infection after viral DNA replication (see for example, 32, 45). Furthermore, both positive and negative feedback mechanisms control the expression of E1A (73), and thus the E1A protein levels in infected cells become stabilized after initial increase. GCA enhanced the expression of HAdV-C5 13S and 12S protein products at 5 h pi, and accelerated appearance of the 9S product at 5 and 9 h pi (Fig. 3 A). In contrast, E1A levels in 293T cells, which harbor an integrated copy of the E1A region (15, 38) were not enhanced but rather reduced by GCA, yet GCA boosted HAdV-C5-dE1_GFP infection in these cells, albeit less efficiently than in A549 cells (Fig. 3 B, C). Further, GCA boosted the expression of the late viral protein VI in HAdV-C5 infected A549 cells by about 30% at 18 h pi compared to untreated cells (Fig. 3 D). GCA treatment resulted in enhanced viral titers 40 h pi both within cells and the extracellular medium (Fig. 3 E). Together, the data indicate that GCA enhances early and late viral gene products from extrachromosomal DNA in context of viral infection, rather than chromosomal DNA, and accelerates the formation of viral progeny.

GCA enhances cancer cell killing

We next tested whether inhibition of GBF-1 boosts HAdV infection of primary tumor stage III melanoma cultures M950822 and M980928, which are both CAR-positive (47, 55). GCA enhanced HAdV-C5-dE1_GFP infection several fold in both cases but had little effects in normal human WI38 fibroblasts (Fig. 4 A). GCA boosted the HAdV-C2-dE3B_GFP infection spread in M980928 cells measured by increase in number of infected cells at 48 h compared to 72 h pi in a live cell assay (Fig. 4 B). Crystal violet cell staining of HAdV-C5_wt infected M950822 and M980928 cells at 72 h pi also indicated that virus cytotoxicity was enhanced by the GCA pretreatment (Fig. 4 C).

To corroborate these results, we measured virus-induced changes to cell phenotypes by recording the impedance at the cell substrate interface using

xCELLigence^{TM}. Changes in impedance, also dubbed cell index (CI) can be measured in real time and label-free, and are proportional to parameters like cell adhesion, proliferation, cell–cell interactions, and cytotoxicity (58, 59). CI dropped as a linear function of log (MOI) upon infection with HAdV-C5_wt, but independent of the initial number of cells on the substrate (Fig. 5 A). The replication-defective HAdV-C5_dE1_GFP had less effects on CI than HAdV-C5_wt, and GCA pretreatment reduced the CI of HAdV-C5_wt infected A549 cells but had essentially no effects on CI of uninfected cells (Fig. 5 B, C). The CI measurements were corroborated by differential interference contrast (DIC) microscopy showing intact monolayers of uninfected cells and progressively rounded cells upon infection with HAdV-C5_wt and GCA treatment (Fig. 5 D, E, F). Note that the increase in number of attached cells 0-40 h post-seeding correlated with an increase in CI values (compare red and blue lines in Fig. 5F). The numbers of attached cells leveled off 40 h post seeding, but the CI values continued to rise up to 50 h post seeding. Both the number of attached cells and CI values remained relatively constant from 75 h onwards in the case of uninfected cells or cells infected with the non-replicating HAdV-C5-dE1_GFP. In the case of HAdV-C5_wt infection both the CI and the amount of attached cells decreased after 85 h. Taking the CI value at 50 h as 100%, a 50% reduction in the CI was reached at ~100 h.

In good agreement, manual counting indicated an equal distribution of rounded-off and attached cells at ~125 h. The sensitivity of cell viability measurements depends on the slope of dip in CI profile, a measure for attached cells. A steep slope of the CI profiles compared to a gradual slope obtained by cell counting indicated a higher sensitivity of xCELLigence to measure cytopathic effects compared to microscopic inspection. Importantly, the CI values of HAdV-C5_wt infection were strongly reduced in GCA treated cancer cells, including M950822 and M980928 melanoma cells, but not in normal WI38 cells compared to control-infected cells, as indicated by negative ΔCIT_{50} values for A549 and melanoma cells in Fig. 5 G. Notably the ΔCIT_{50} values correlated well with HAdV-C5-dE1_GFP infection phenotype (Fig. 5 G), and confirmed the strong acceleration of HAdV infection by GCA.

Contrary to HAdV infection, GCA increased the CIT values from human rhinovirus (HRV) A1A infections indicating reduced cytopathic effects, in good correlation with infection reduction (Fig. 5 H, I, J). This result was in agreement with the notions that GCA blocks replication of HRV related enteroviruses by dissociating Arf1 and COP-I

from Golgi membranes (69), and that HRV-A1A requires lipid flux between the ER and Golgi for replication (51).

IRE-1 and XBP-1 are required for GCA enhancement of HAdV infection

UPR enhances the protein folding capacity in the ER upon stress conditions, such as physical, chemical or biological insults, developmental processes or cancer (6). ER stress activates three signaling arms of UPR, IRE-1/XBP-1, PKR-like ER kinase (PERK) and ATF-6 (37). This can lead to cell protection or cell death. The former is favored by the IRE-1 branch, and the latter by the ATF-6 and PERK arms (37). Since knockdown of GBF-1 has been shown to induce the ATF-6 arm of the UPR (11), we tested whether the UPR was linked to the GCA boost of HAdV infection. The knock-down of IRE-1alpha with a pool of four siRNAs had the strongest effect on blunting GCA enhancement, although ATF-6B knock-down reduced the boost as well (Fig. 6 A). We confirmed these results with a pool of 30 synthetic siRNAs (siP-RNAs), which were reported to have no detectable off-target effects (26). The siP-IRE-1 RNAs blocked infection boost and reduced the IRE-1 protein levels (Fig. 6 B). The treatment of cells with GCA triggered the IRE-1/XBP-1 branch of the UPR, similar to the ER stress activator thapsigargin, as indicated by the activation of cytoplasmic splicing of XBP-1 mRNA, and this splicing was inhibited by the IRE-1 nuclease inhibitor 4μ8C (Fig. 6 C, 13). Similar to GCA, thapsigargin boosted HAdV-C5-dE1_GFP infection, and 4μ8C blunted both the GCA and thapsigargin boosts (Fig. 6 D). For HAdV-C5-dE1_GFP, the GCA infection boost was strongly, but not completely reduced in XBP-1 knock-out mouse embryo fibroblasts (36), akin to XBP-1 siP-RNA treated A549 cells (Fig. 6 E, F), suggesting a major, though not exclusive role of XBP-1 in boosting infection.

The involvement of the IRE-1/XBP-1 branch in the GCA infection boost was further tested by live cell assays measuring infection spreading, where ‘comets’ of infected cells are formed by replicating HAdV-C2-dE3B_GFP (72). Comets are the equivalent of plaques, but obtained in the absence of gelling medium. They consist of dozens of GFP-positive cells in an elongated arrangement due to convection flow of cell-free viruses from lytic infected cells. GCA enhanced the formation of comets in a time-dependent manner (Fig. 7 A, B). Importantly, siP-RNAs against IRE-1 or XBP-1 blunted the GCA enhancement of comet formation (Fig. 7 C, D). Notably,

these siP-RNAs reduced the number of comets also without GCA treatment, implying that IRE-1 and XBP-1 contribute to the replication of HAdV in the absence of exogenous UPR stimulation.

DISCUSSION

IRE-1 senses unfolded proteins in the ER lumen, and this activates the IRE-1 cytosolic kinase and endonuclease functions, and leads to splicing of XBP-1 mRNA yielding a transcript, which encodes the active XBP-1 transcription factor (64). XBP-1 alleviates ER stress. We show here that the inhibition of the Arf-activator GBF-1 by GCA induced the IRE-1/XBP-1 branch of the UPR (summarized in a model presented in Fig. 8). Chemical induction of the UPR boosted HAdV-C5 or B3 infections, specifically in cancer cells. This may have therapeutic relevance, since the CAR-tropic HAdV-C5 is used to treat metastatic tumors, and the CD46/DSG-2 tropic HAdV-B3 late stage cancers with down-regulated CAR, for example prostate cancer (50). Importantly, UPR is readily inducible in aggressive tumor cells, and promotes survival, angiogenesis, autophagy, epithelial-mesenchymal transition (EMT) or adaptation to hypoxic conditions. While angiogenesis, EMT and hypoxia adaptation depend on the PERK branch, the XBP-1 branch supports some forms of breast cancer (9, 18, 52). We expect that cells with fast or strong induction of IRE-1/XBP-1 will enhance HAdV infection particularly well, while cells with low or slow induction will show a lesser infection boost upon chemical UPR induction. But in both cases, cancer cells can be killed by HAdV.

On a mechanistic level, our results demonstrate that knockdown or inhibition of GBF-1 by GCA enhanced early viral and transgene expressions from adenovirus, enhanced late gene expression and cytopathic effects, formation and release of progeny from infected cells and enhanced virus spreading to neighboring cells. This cascade of effects boosted cancer cell killing. It was to a large extent dependent on the ability of GCA to induce the IRE-1/XBP-1 branch of the UPR. Interestingly, the GCA effects were not limited to wild type HAdV, but occurred also with replication-defective HAdV expressing a transgene under the major immediate early CMV

promoter. Like for HAdV-C5_wt, this enhancement required IRE-1/XBP-1 suggesting that this UPR branch acts on the E1A and the CMV promoters. However, promoter mechanisms are not sufficient to induce the viral infection boost, since GCA did not enhance gene expression from transfected plasmid DNA or chromosomally integrated viral E1 DNA. Furthermore, our results also indicate that GCA did not enhance virus binding to cells. We speculate that viral insults to cell integrity during entry enhance infection together with elements of the IRE-1/XBP-1 pathway. This combined action may enhance nuclear import of the viral genome, affect the structure or protein composition of the viral genome in the nucleus, or involve epigenetic regulatory machineries (2, 31, 56, 70). Since UPR induction enhanced both the GFP expression from HAdV-C5-dE1_GFP and E1A or GFP expression from a replicating HAdV-C, this suggests that some early event in virus life cycle is targeted. However, whether this as-yet-unidentified early effect also fully explains the accelerated spreading of virus infection or whether infection is accelerated / enhanced by more than one mechanism is at present unclear. Furthermore, the exact molecular mechanism(s) by which IRE-1/XBP-1 enhance the HAdV infections is still unclear. This could involve one or more cellular (or viral) genes induced by XBP-1.

The approach outlined here allows for the identification of host pathways boosting infection with viral vectors in any cell type of interest. Specifically, the cell impedance measurements can score cytopathic effects of virus infections in real time, and label-free, and can identify both infection enhancing and inhibiting compounds in semi-high throughput format without the need of constructing specific reporter viruses. Boosters of viral infection are needed to enhance and tune the efficacy of oncolytic virotherapies. Potential signaling branches downstream of the IRE-1 UPR node triggered by the small chemical GCA to enhance cancer cell killing are discussed in Fig. 8. Oncolytic therapies kill cancer cells, lead to inflammation, and ideally present tumor-associated antigens to immune cells to mount immune responses against tumors (43, 44). Viral oncolysis also crucially depends on efficient intratumoral transmission of the oncolytic agents, and the ability of the virus to overcome innate immunity (28). Notably, the spreading of HAdV-C occurs by cell-free viruses after lysis of infected cells. Yet, spreading and oncolysis are limited both in cell cultures and organisms (27, 72). Our data raise the possibility to chemically tune viral oncolysis by manipulating the UPR, and apply this for cancer treatment.

AUTHORS CONTRIBUTIONS

Designed and performed experiments (VP, MS, MP), interpreted data (VP, MS, AY, VA, SH, UFG), wrote manuscript (VP, MS, UFG), coordinated study (UFG).

ACKNOWLEDGEMENTS

We thank Laurie Glimcher and Ann-Hwee Lee (Weill Cornell Medical College, NY, USA) for XBP-1 MEFs, and Daria Mudrak, Bettina Cardel (University of Zurich, Switzerland) and Wai-Ming Lee (University of Wisconsin, Madison, Wisconsin, USA) for supplying HRV-A1A and anti-VP2 hybridoma antibody. The work was supported by the Swiss National Science Foundation (Grant 31003A_141222/1), and an Initial Training Network grant 'AdVance' from the European Union to UFG.

CONFLICT OF INTEREST

The authors declare that they have no conflict of interest.

REFERENCES

1. **Bell, J., and G. McFadden.** 2014. Viruses for Tumor Therapy. Cell Host Microbe **15:**260-265.

2. **Berscheminski, J., P. Groitl, T. Dobner, P. Wimmer, and S. Schreiner.** 2013. The adenoviral oncogene E1A-13S interacts with a specific isoform of the tumor suppressor PML to enhance viral transcription. Journal of virology **87:**965-977.

3. **Bovenberg, M. S., M. H. Degeling, and B. A. Tannous.** 2013. Advances in stem cell therapy against gliomas. Trends Mol Med **19:**281-291.

4. **Bremner, K. H., J. Scherer, J. Yi, M. Vershinin, S. P. Gross, and R. B. Vallee.** 2009. Adenovirus transport via direct interaction of cytoplasmic dynein with the viral capsid hexon subunit. Cell Host Microbe **6:**523-535.

5. **Burckhardt, C. J., M. Suomalainen, P. Schoenenberger, K. Boucke, S. Hemmi, and U. F. Greber.** 2011. Drifting motions of the adenovirus receptor CAR and immobile integrins initiate virus uncoating and membrane lytic protein exposure. Cell Host Microbe **10:**105-117.

6. **Calfon, M., H. Zeng, F. Urano, J. H. Till, S. R. Hubbard, H. P. Harding, S. G. Clark, and D. Ron.** 2002. IRE1 couples endoplasmic reticulum load to secretory capacity by processing the XBP-1 mRNA. Nature **415:**92-96.

7. **Carpenter, A. E., T. R. Jones, M. R. Lamprecht, C. Clarke, I. H. Kang, O. Friman, D. A. Guertin, J. H. Chang, R. A. Lindquist, J. Moffat, P. Golland, and D. M. Sabatini.** 2006. CellProfiler: image analysis software for identifying and quantifying cell phenotypes. Genome Biol **7:**R100.

8. **Chen, D. S., and I. Mellman.** 2013. Oncology meets immunology: the cancer-immunity cycle. Immunity **39:**1-10.

9. **Chen, X., D. Iliopoulos, Q. Zhang, Q. Tang, M. B. Greenblatt, M. Hatziapostolou, E. Lim, W. L. Tam, M. Ni, Y. Chen, J. Mai, H. Shen, D. Z. Hu, S. Adoro, B. Hu, M. Song, C. Tan, M. D. Landis, M. Ferrari, S. J. Shin, M. Brown, J. C. Chang, X. S. Liu, and L. H. Glimcher.** 2014. XBP1 promotes triple-negative breast cancer by controlling the HIF1alpha pathway. Nature **508:**103-107.

10. **Cho, J. A., A. H. Lee, B. Platzer, B. C. Cross, B. M. Gardner, H. De Luca, P. Luong, H. P. Harding, L. H. Glimcher, P. Walter, E. Fiebiger, D. Ron, J. C. Kagan, and W. I. Lencer.** 2013. The Unfolded Protein Response Element IRE1alpha Senses Bacterial Proteins Invading the ER to Activate RIG-I and Innate Immune Signaling. Cell Host Microbe **13:**558-569.

11. **Citterio, C., A. Vichi, G. Pacheco-Rodriguez, A. M. Aponte, J. Moss, and M. Vaughan.** 2008. Unfolded protein response and cell death after depletion of brefeldin A-inhibited guanine nucleotide-exchange protein GBF1. Proc Natl Acad Sci U S A **105:**2877-2882.

12. **Claude, A., B.-P. Zhao, C. E. Kuziemsky, S. Dahan, S. J. Berger, J.-P. Yan, A. D. Armold, E. M. Sullivan, and P. Melançon.** 1999. Gbf1 A Novel

Golgi-Associated Bfa-Resistant Guanine Nucleotide Exchange Factor That Displays Specificity for Adp-Ribosylation Factor 5. The Journal of cell biology **146:**71-84.

13. **Cross, B. C., P. J. Bond, P. G. Sadowski, B. K. Jha, J. Zak, J. M. Goodman, R. H. Silverman, T. A. Neubert, I. R. Baxendale, D. Ron, and H. P. Harding.** 2012. The molecular basis for selective inhibition of unconventional mRNA splicing by an IRE1-binding small molecule. Proc Natl Acad Sci U S A **109:**E869-878.

14. **Dazard, J.-E., K. Zhang, J. Sha, O. Yasin, L. Cai, C. Nguyen, M. Ghosh, J. Bongorno, and M. L. Harter.** 2011. The dynamics of E1A in regulating networks and canonical pathways in quiescent cells. BMC research notes **4:**160.

15. **DuBridge, R. B., P. Tang, H. C. Hsia, P. M. Leong, J. H. Miller, and M. P. Calos.** 1987. Analysis of mutation in human cells by using an Epstein-Barr virus shuttle system. Mol Cell Biol **7:**379-387.

16. **Fallaux, F. J., O. Kranenburg, S. J. Cramer, A. Houweling, H. van Ormondt, R. C. Hoeben, and A. J. van der Eb.** 1996. Characterization of 911: a new helper cell line for the titration and propagation of early region 1-deleted adenoviral vectors. Human gene therapy **7:**215-222.

17. **Fejer, G., L. Drechsel, J. Liese, U. Schleicher, Z. Ruzsics, N. Imelli, U. F. Greber, S. Keck, B. Hildenbrand, A. Krug, C. Bogdan, and M. A. Freudenberg.** 2008. Key role of splenic myeloid DCs in the IFN-alphabeta response to adenoviruses in vivo. PLoS Pathog **4:**e1000208.

18. **Feng, Y. X., E. S. Sokol, C. A. Del Vecchio, S. Sanduja, J. H. Claessen, T. A. Proia, D. X. Jin, F. Reinhardt, H. L. Ploegh, Q. Wang, and P. B. Gupta.** 2014. Epithelial-to-Mesenchymal Transition Activates PERK-eIF2alpha and Sensitizes Cells to Endoplasmic Reticulum Stress. Cancer discovery **4:**702-715.

19. **Fleischli, C., D. Sirena, G. Lesage, M. J. Havenga, R. Cattaneo, U. F. Greber, and S. Hemmi.** 2007. Species B adenovirus serotypes 3, 7, 11 and 35 share similar binding sites on the membrane cofactor protein CD46 receptor. J Gen Virol **88:**2925-2934.

20. **Ginn, S. L., I. E. Alexander, M. L. Edelstein, M. R. Abedi, and J. Wixon.** 2013. Gene therapy clinical trials worldwide to 2012 - an update. J Gene Med **15:**65-77.

21. **Greber, U. F., N. Arnberg, G. Wadell, M. Benko, and E. J. Kremer.** 2013. Adenoviruses - from pathogens to therapeutics: a report on the 10th International Adenovirus Meeting. Cell Microbiol **15:**16-23.

22. **Greber, U. F., P. Webster, J. Weber, and A. Helenius.** 1996. The role of the adenovirus protease on virus entry into cells. EMBO J **15:**1766-1777.

23. **Greber, U. F., M. Willetts, P. Webster, and A. Helenius.** 1993. Stepwise dismantling of adenovirus 2 during entry into cells. Cell **75:**477-486.

24. **Han, D., A. G. Lerner, L. Vande Walle, J.-P. Upton, W. Xu, A. Hagen, B. J. Backes, S. A. Oakes, and F. R. Papa.** 2009. IRE1α kinase activation modes control alternate endoribonuclease outputs to determine divergent cell fates. Cell **138:**562-575.

25. **Hanahan, D., and R. A. Weinberg.** 2011. Hallmarks of cancer: the next generation. Cell **144:**646-674.

26. **Hannus, M., M. Beitzinger, J. C. Engelmann, M. T. Weickert, R. Spang, S. Hannus, and G. Meister.** 2014. siPools: highly complex but accurately defined siRNA pools eliminate off-target effects. Nucleic Acids Res **42:**8049-8061.

27. **Hemminki, O., I. Diaconu, V. Cerullo, S. K. Pesonen, A. Kanerva, T. Joensuu, K. Kairemo, L. Laasonen, K. Partanen, L. Kangasniemi, A. Lieber, S. Pesonen, and A. Hemminki.** 2012. Ad3-hTERT-E1A, a fully serotype 3 oncolytic adenovirus, in patients with chemotherapy refractory cancer. Mol Ther **20:**1821-1830.

28. **Hendrickx, R., N. Stichling, J. Koelen, L. Kuryk, A. Lipiec, and U. F. Greber.** 2014. Innate Immunity to Adenovirus. Hum Gene Ther **25:**265–284.

29. **Hetz, C., F. Martinon, D. Rodriguez, and L. H. Glimcher.** 2011. The unfolded protein response: integrating stress signals through the stress sensor IRE1alpha. Physiol Rev **91:**1219-1243.

30. **Hollien, J., J. H. Lin, H. Li, N. Stevens, P. Walter, and J. S. Weissman.** 2009. Regulated Ire1-dependent decay of messenger RNAs in mammalian cells. J Cell Biol **186:**323-331.

31. **Horwitz, G. A., K. Zhang, M. A. McBrian, M. Grunstein, S. K. Kurdistani, and A. J. Berk.** 2008. Adenovirus small e1a alters global patterns of histone modification. Science **321:**1084-1085.

32. **Hu, M. C., and M. T. Hsu.** 1997. Adenovirus E1B 19K protein is required for efficient DNA replication in U937 cells. Virology **227:**295-304.

33. **Jurgeit, A., R. McDowell, S. Moese, E. Meldrum, R. Schwendener, and U. F. Greber.** 2012. Niclosamide is a proton carrier and targets acidic endosomes with broad antiviral effects. PLoS Pathog **8:**e1002976; 1002910.1001371/journal.ppat.1002976.

34. **Jurgeit, A., S. Moese, P. Roulin, A. Dorsch, M. Lotzerich, W. M. Lee, and U. F. Greber.** 2010. An RNA replication-center assay for high content image-based quantifications of human rhinovirus and coxsackievirus infections. Virol J **7:**264.

35. **Kyula, J. N., A. A. Khan, D. Mansfield, E. M. Karapanagiotou, M. McLaughlin, V. Roulstone, S. Zaidi, T. Pencavel, Y. Touchefeu, R. Seth, N. G. Chen, Y. A. Yu, Q. Zhang, A. A. Melcher, R. G. Vile, H. S. Pandha, M. Ajaz, A. A. Szalay, and K. J. Harrington.** 2014. Synergistic cytotoxicity of radiation and oncolytic Lister strain vaccinia in (V600D/E)BRAF mutant melanoma depends on JNK and TNF-alpha signaling. Oncogene **33:**1700-1712.

36. **Lee, A. H., N. N. Iwakoshi, and L. H. Glimcher.** 2003. XBP-1 regulates a subset of endoplasmic reticulum resident chaperone genes in the unfolded protein response. Mol Cell Biol **23:**7448-7459.

37. **Lin, J. H., H. Li, D. Yasumura, H. R. Cohen, C. Zhang, B. Panning, K. M. Shokat, M. M. Lavail, and P. Walter.** 2007. IRE1 signaling affects cell fate during the unfolded protein response. Science **318:**944-949.

38. **Louis, N., C. Evelegh, and F. L. Graham.** 1997. Cloning and sequencing of the cellular-viral junctions from the human adenovirus type 5 transformed 293 cell line. Virology **233:**423-429.

39. **Lutschg, V., K. Boucke, S. Hemmi, and U. F. Greber.** 2011. Chemotactic antiviral cytokines promote infectious apical entry of human adenovirus into polarized epithelial cells. Nat Commun **2:**391.

40. **Mahoney, D. J., C. Lefebvre, K. Allan, J. Brun, C. A. Sanaei, S. Baird, N. Pearce, S. Gronberg, B. Wilson, M. Prakesh, A. Aman, M. Isaac, A. Mamai, D. Uehling, R. Al-Awar, T. Falls, T. Alain, and D. F. Stojdl.** 2011. Virus-tumor interactome screen reveals ER stress response can reprogram resistant cancers for oncolytic virus-triggered caspase-2 cell death. Cancer Cell **20:**443-456.

41. **Mansour, S. J., J. A. Herbrick, S. W. Scherer, and P. Melancon.** 1998. Human GBF1 is a ubiquitously expressed gene of the sec7 domain family mapping to 10q24. Genomics **54:**323-327.

42. **Marciniak, S. J., C. Y. Yun, S. Oyadomari, I. Novoa, Y. Zhang, R. Jungreis, K. Nagata, H. P. Harding, and D. Ron.** 2004. CHOP induces death by promoting protein synthesis and oxidation in the stressed endoplasmic reticulum. Genes Dev **18:**3066-3077.

43. **Mellman, I., G. Coukos, and G. Dranoff.** 2011. Cancer immunotherapy comes of age. Nature **480:**480-489.

44. **Miest, T. S., and R. Cattaneo.** 2014. New viruses for cancer therapy: meeting clinical needs. Nat Rev Microbiol **12:**23-34.

45. **Miller, M. S., P. Pelka, G. J. Fonseca, M. J. Cohen, J. N. Kelly, S. D. Barr, R. J. Grand, A. S. Turnell, P. Whyte, and J. S. Mymryk.** 2012. Characterization of the 55-residue protein encoded by the 9S E1A mRNA of species C adenovirus. J Virol **86:**4222-4233.

46. **Moyer, C. L., C. M. Wiethoff, O. Maier, J. G. Smith, and G. R. Nemerow.** 2011. Functional genetic and biophysical analyses of membrane disruption by human adenovirus. J Virol **85:**2631-2641.

47. **Nagel, H., S. Maag, A. Tassis, F. O. Nestle, U. F. Greber, and S. Hemmi.** 2003. The alphavbeta5 integrin of hematopoietic and nonhematopoietic cells is a transduction receptor of RGD-4C fiber-modified adenoviruses. Gene Ther **10:**1643-1653.

48. **Pelka, P., J. N. Ablack, G. J. Fonseca, A. F. Yousef, and J. S. Mymryk.** 2008. Intrinsic structural disorder in adenovirus E1A: a viral molecular hub linking multiple diverse processes. Journal of virology **82:**7252-7263.

49. **Puntener, D., M. F. Engelke, Z. Ruzsics, S. Strunze, C. Wilhelm, and U. F. Greber.** 2011. Stepwise loss of fluorescent core protein V from human adenovirus during entry into cells. J Virol **85:**481-496.

50. **Rauen, K. A., D. Sudilovsky, J. L. Le, K. L. Chew, B. Hann, V. Weinberg, L. D. Schmitt, and F. McCormick.** 2002. Expression of the coxsackie adenovirus receptor in normal prostate and in primary and metastatic prostate carcinoma: potential relevance to gene therapy. Cancer Res **62:**3812-3818.

51. **Roulin, P., M. Lotzerich, L. B. Tanner, F. T. Torta, F. van Kuppefeld, M. R. Wenk, and U. F. Greber.** 2014. A Phosphatidylinositol 4-Phosphate and Cholesterol Counter-Current Model for the Formation of Rhinovirus Replication Compartments at ER-Golgi Interface. Cell Host & Microbes, in revision.

52. **Rouschop, K. M., T. van den Beucken, L. Dubois, H. Niessen, J. Bussink, K. Savelkouls, T. Keulers, H. Mujcic, W. Landuyt, J. W. Voncken, P. Lambin, A. J. van der Kogel, M. Koritzinsky, and B. G. Wouters.** 2010. The unfolded protein response protects human tumor cells during hypoxia through regulation of the autophagy genes MAP1LC3B and ATG5. J Clin Invest **120:**127-141.

53. **Russell, S. J., K. W. Peng, and J. C. Bell.** 2012. Oncolytic virotherapy. Nat Biotechnol **30:**658-670.

54. **Saenz, J. B., W. J. Sun, J. W. Chang, J. Li, B. Bursulaya, N. S. Gray, and D. B. Haslam.** 2009. Golgicide A reveals essential roles for GBF1 in Golgi assembly and function. Nat Chem Biol **5:**157-165.

55. **Schmitz, M., C. Graf, T. Gut, D. Sirena, I. Peter, R. Dummer, U. F. Greber, and S. Hemmi.** 2006. Melanoma cultures show different susceptibility towards E1A-, E1B-19 kDa- and fiber-modified replication-competent adenoviruses. Gene Ther **13:**893-905.

56. **Schreiner, S., S. Kinkley, C. Bürck, A. Mund, P. Wimmer, T. Schubert, P. Groitl, H. Will, and T. Dobner.** 2013. SPOC1-mediated antiviral host cell response is antagonized early in human adenovirus type 5 infection. PLoS pathogens **9:**e1003775.

57. **Sirena, D., Z. Ruzsics, W. Schaffner, U. F. Greber, and S. Hemmi.** 2005. The nucleotide sequence and a first generation gene transfer vector of species B human adenovirus serotype 3. Virology **343:**283-298.

58. **Solly, K., X. Wang, X. Xu, B. Strulovici, and W. Zheng.** 2004. Application of real-time cell electronic sensing (RT-CES) technology to cell-based assays. Assay and drug development technologies **2:**363-372.

59. **Spiegel, M.** 2009. Real-time and Dynamic Monitoring of Virus-mediated Cytopathogenicity, p. 15-17, vol. 3. Biochemica.

60. **Strunze, S., M. F. Engelke, I.-H. Wang, D. Puntener, K. Boucke, S. Schleich, M. Way, P. Schoenenberger, C. J. Burckhardt, and U. F. Greber.** 2011. Kinesin-1-mediated capsid disassembly and disruption of the nuclear pore complex promote virus infection. Cell Host Microbe **10:**210-223.

61. **Suomalainen, M., S. Luisoni, K. Boucke, S. Bianchi, D. A. Engel, and U. F. Greber.** 2013. A direct and versatile assay measuring membrane penetration of adenovirus in single cells. J Virol **87:**12367-12379.

62. **Suomalainen, M., M. Y. Nakano, K. Boucke, S. Keller, R. P. Stidwill, and U. F. Greber.** 1999. Microtubule-dependent minus and plus end-directed motilities are competing processes for nuclear targeting of adenovirus. J. Cell Biol. **144:**657-672.

63. **Szul, T., R. Garcia-Mata, E. Brandon, S. Shestopal, C. Alvarez, and E. Sztul.** 2005. Dissection of membrane dynamics of the ARF-guanine nucleotide exchange factor GBF1. Traffic **6:**374-385.

64. **Tirasophon, W., A. A. Welihinda, and R. J. Kaufman.** 1998. A stress response pathway from the endoplasmic reticulum to the nucleus requires a novel bifunctional protein kinase/endoribonuclease (Ire1p) in mammalian cells. Genes Dev **12:**1812-1824.

65. **Toth, K., D. Dhar, and W. S. Wold.** 2010. Oncolytic (replication-competent) adenoviruses as anticancer agents. Expert Opin Biol Ther **10:**353-368.

66. **Toth, K., and W. S. Wold.** 2010. Increasing the efficacy of oncolytic adenovirus vectors. Viruses **2:**1844-1866.

67. **Touchefeu, Y., P. Franken, and K. J. Harrington.** 2012. Radiovirotherapy: principles and prospects in oncology. Curr Pharm Des **18:**3313-3320.

68. **Upton, J. P., L. Wang, D. Han, E. S. Wang, N. E. Huskey, L. Lim, M. Truitt, M. T. McManus, D. Ruggero, A. Goga, F. R. Papa, and S. A. Oakes.** 2012. IRE1alpha cleaves select microRNAs during ER stress to derepress translation of proapoptotic Caspase-2. Science **338:**818-822.

69. **van der Linden, L., H. M. van der Schaar, K. H. Lanke, J. Neyts, and F. J. van Kuppeveld.** 2010. Differential effects of the putative GBF1 inhibitors Golgicide A and AG1478 on enterovirus replication. J Virol **84:**7535-7542.

70. **Wang, I. H., M. Suomalainen, V. Andriasyan, S. Kilcher, J. Mercer, A. Neef, N. W. Luedtke, and U. F. Greber.** 2013. Tracking viral genomes in host cells at single-molecule resolution. Cell Host Microbe **14:**468-480.

71. **Wolfrum, N., and U. F. Greber.** 2013. Adenovirus signalling in entry. Cell Microbiol **15:**53-62.

72. **Yakimovich, A., H. Gumpert, C. J. Burckhardt, V. A. Lutschg, A. Jurgeit, I. F. Sbalzarini, and U. F. Greber.** 2012. Cell-free transmission of human adenovirus by passive mass transfer in cell culture simulated in a computer model. Journal of Virology **86:**10123–10137.

73. **Yoshida, K., F. Higashino, and K. Fujinaga.** 1995. Transcriptional regulation of the adenovirus E1A gene, p. 113-130, The Molecular Repertoire of Adenoviruses III. Springer.

74. **Zhao, X., A. Claude, J. Chun, D. Shields, J. Presley, and P. Melançon.** 2006. GBF1, a cis-Golgi and VTCs-localized ARF-GEF, is implicated in ER-to-Golgi protein traffic. Journal of Cell Science **119:**3743-3753.

FIGURE LEGENDS

Figure 1: Knockdown of GBF-1 enhances HAdV infections

(A) RNA interference mini-screen against Arf-GEFs identifies GBF-1 knock-down as an enhancer of HAdV-C5-dE1_GFP, HAdV-C5_wt and HAdV-C2-dE3B_GFP infections. Cells were reverse transfected with pooled siRNAs (1 pmol/well) against cytohesin (CYTH)-1, CYTH-2, CYTH-3, Brefeldin A-inhibited guanine nucleotide-exchange protein (BIG)-1, BIG2 or GBF-1 for 48 h, infected as indicated, fixed 18 h pi, and analyzed for infection. Results are expressed as log 10 ratio of infected cells (mean nuclear intensity of GFP) normalized to control cells transfected with nontargeting siRNA.

(B, C, D) Knockdown of GBF-1 siRNA enhances HAdV-C5-dE1_GFP infection in A549 cells. Single or pooled GBF-1 siRNAs, along with control non-targeting (NT), Kif11 (Kinesin family member protein 11) siRNAs and GFP siRNAs were reverse transfected into A549 cells and cells were infected 48h post transfection. Eighteen hours post infection cells were fixed, stained with DAPI and analyzed for infection. (B) shows representative images. Scale bar is 100µm. (C) shows quantification of GFP signal in cells transfected with the indicated siRNAs. RU=relative units represent mean nuclear GFP signal from three parallel samples ± SDs. The cell toxicity of the siRNAs was measured with the cell number shown on secondary x-axis.

Figure 2: Prolonged inhibition of GBF-1 enhances HAdV infection in A549 cells, but not virus binding to cells

(A) Dispersal of Golgi upon treatment of A549 cells with GBF-1 inhibitor GCA for 30 min. Cells were fixed and immunostained with antibodies directed against the Golgi-associated protein giantin (green) and nuclei (blue) were stained with DAPI. Samples were imaged by confocal fluorescence microscopy. Images show maximum projections of confocal sections. Note that control DMSO-treated cells showed normal peri-nuclear Golgi staining. Five µM GCA had no effect, 10 µM caused incomplete disruption of Golgi, and 20 µM induced efficient disruption of Golgi in all cells. Scale bar 20 µm.

(B) Minor effect of GCA on metabolic activity of A549 cells. Cells were treated with GCA or control DMSO for 5 h, and the metabolic activity in cells was measured by resazurin fluorescence assay (RFU=relative fluorescence unit).

(C) Five-hour pre-incubation with GCA is sufficient to enhance HAdV-C5-dE1_GFP infection of A549 cells. Cells were pre-incubated with GCA or DMSO for 5 h, inoculated with HAdV-C5-dE1_GFP and infection was carried out in presence or absence of GCA. Cells were fixed 18h pi and mean nuclear intensity of GFP was used to score infection efficiency (RU= relative units). A graphical representation of the experiment is shown on the left, experimental results with mean values from three parallel experiments +/- SD on the right.

(D) Five-hour pre-incubation with GCA enhances HAdV-C5-dE1_GFP, HAdV-C2_dE1_GFP and HAdV-B3-dE1_GFP infection in A549 cells.

(E) GCA has no effect on a plasmid-mediated CMV promoter-driven GFP expression. A549 cells were transfected with pMAX-GFP plasmid, 24 h post transfection treated with GCA for 5h, and analyzed for GFP expression 5 or 21 h post drug removal.

(F) Decrease in atto565-labelled HAdV-C5 attachment to A549 cells upon GCA treatment. Cells were treated with GCA for 12 or 0.5 h followed by inoculation with atto565-labelled HAdV-C5_wt at cold for 30 min, washing and 5 min pulse at 37°C. Number of virus particles in individual cells was determined from maximum intensity projections of confocal stacks using a custom made Matlab^{TM} script. One dot represents one cell. Error bars represent the means ± SEMs and p-values were calculated using Mann-Whitney test for statistics.

(G) Acute inhibition of GBF-1 upon virus addition does not enhance HAdV-C5-dE1_GFP infection in A549 cells. GCA or DMSO was added to cells 30 min prior to virus or as indicated pi, and incubation was continued until 18 h pi, when cells were analyzed.

Figure 3: Inhibition of GBF-1 by GCA enhances HAdV-C early and late gene expression, as well as virus production in A549 cells.

(A) Five-hour pre-incubation with GCA accelerates E1A expression from HAdV-C5 wild type in A549 cells, as indicated by Western blotting of infected cell lysates. E1A forms encoded by the differentially spliced E1A transcripts are indicated. Lower panel shows the β-tubulin loading control.

(B) GCA does not increase E1A levels in uninfected 293T cells, which express E1A from a chromosomal copy. Cell extracts were prepared after 5h incubation with DMSO or GCA, and E1A levels were determined by immunoblot using β-tubulin as a loading control.

(C) GCA boosts HAdV-C5-dE1_GFP infection in 293T cells. Cells were pre-incubated with GCA for 5 h, inoculated with virus and analyzed for GFP expression 18 h pi.

(D) GBF-1 inhibition enhances expression of the late protein VI in A549 cells. Cells were pre-incubated with GCA for 5h, infected with HAdV-C5-wt and analyzed for protein VI expression 18h pi. Left panel shows representative images (green protein VI signal and blue DAPI signal). Scale bar 100µm. Right-hand panel shows quantification of average nuclear protein VI signal (RU=relative units).

(E) Inhibition of GBF-1 accelerates the production and release of HAdV-C2-dE3B_GFP in A549 cells 40 h pi. Cells were pre-incubated with DMSO or GCA for 5h, inoculated with the virus (MOI 0.008) and 40 h pi progeny particles were collected from cells and culture supernatants. Titers of the cell-associated and supernatant fractions were determined on HeLa-ATCC cells by counting GFP positive cells 18 h pi.

Figure 4: GBF-1 inhibition enhances adenovirus infection of melanoma cells

(A) Inhibition of GBF-1 by GCA enhances HAdV-C5-dE1_GFP infection of M950822 and M980928 melanoma cells, but not normal human WI38 fibroblasts. Cells were pre-incubated with DMSO or GCA for 5h, inoculated with the virus and analyzed 18 h pi. Shown are representative images and quantification of mean nuclear GFP signal (RU=relative units).

(B) Inhibition of GBF-1 enhances HAdV-C2-dE3B_GFP spreading in melanoma-derived M980928 cells. The cells were pre-incubated with DMSO or GCA for 5 h

and inoculated with the virus (MOI ~ 0.00016). The data is from a live experiment with recordings every 4 h – 5h. Shown is quantification of the number of GFP-positive cells at 48 h and 72 h pi.

(C) Inhibition of GBF-1 enhances HAdV-C5_wt-induced killing of M950822 and M980928 cells. The cells were pre-incubated with DMSO or GCA for 5 h, inoculated with HAdV-C5_wt (MOI 1) and stained with crystal violet 72 h pi. Right-hand panel shows quantification of crystal violet staining, which is proportional to cell numbers.

Figure 5: Inhibition of GBF-1 enhances HAdV-induced cytopathic effects, but blocks rhinovirus infection.

(A) Cell index (CI) profiles from impedance measurements of A549 infected with HAdV-C5_wt indicate cytopathic effects. Impedance was recorded every 15 min using xCELLigence^{TM}. Each point represents the average value from two replicates with SD. Time on x-axis indicates the time post cell seeding. Vertical lines show the time of infection and horizontal lines refer to 50% of the maximum CI of non-infected cells. Right-hand panel shows regression fit of ΔCIT_{50} values, where each point represents a single ΔCIT_{50} value. Note that the CI-profile of HAdV-C5_wt infection is MOI but not cell density dependent.

(B) A549 cells infected with HAdV-C5_wt (red) or replication-deficient HAdV-C5-dE1_GFP (blue) yield significantly different CI profiles. The profile of HAdV-C5-dE1_GFP infected cells is similar to that of non-infected control cells (brown).

(C) Five-hour pre-incubation with GCA enhanced HAdV-C5_wt induced cytotoxicity in A549 cells. Data points represent means from two samples per condition ±SD.

(D) DIC images of control and GCA-treated (5 h pre-incubation) uninfected and HAdV-C5_wt-infected A549 cells 72 h pi. Scale bar 50 µm.

(E, F) Comparison of CI values with cell appearance in DIC images. Panel E shows representative DIC images of A549 cells classified as rounded (1, green), attached (2, blue) or in an intermediate state (3, brown). Scale bar 50 µm. The upper image is unprocessed, whereas the lower image shows an example of images that were band-pass filtered and contrast enhanced using ImageJ. The latter images were used for cell classification. Panel F compares the CI profiles of uninfected, HAdV-

C5-dE1_GFP (MOI 1) and HAdV-C5_wt (MOI 1) infected A549 cells with the number of rounded, attached and intermediate cells in DIC images of corresponding parallel samples. Red line indicates CI, green line the number of rounded cells, blue line the number of attached cells and brown line the number of intermediate cells.

(G) Summary of GCA-mediated infection enhancement for HAdV-C5-dE1_GFP and ΔCIT_{50} values (h) for HAdV-C5_wt. Negative values in the ΔCIT_{50} column indicate that GCA-treated cells reached 50% maximum CI of non-infected cells earlier than control DMSO-treated cells.

(H) GCA inhibits HRV-A1A infection of HeLa-Ohio cells as indicated by anti-VP2 immunostaining. Cells were infected with HRV-A1A (MOI 0.01) in the presence of 20 µM GCA and analyzed for VP2 expression 7h pi. Representative images are shown on the left (VP2 green and DAPI blue) and quantification of cytoplasmic VP2 signal on the right-hand side.

(I) CI profile of HeLa-Ohio cells infected with HRV-A1A at different MOIs. Values are the average of two replicates including SD.

(J) The GBF-1 inhibitor GCA reduced HRV-A1A-induced CPE in HeLa-Ohio cells. Cells were infected with HRV-A1A (MOI 0.01) in the presence of 20 µM GCA. Data represent means ±SD from 2 samples per condition.

Figure 6: GCA enhances adenovirus infection through IRE-1 and XBP-1

(A) Effect of knockdown of ER stress sensors on GCA-mediated infection boost. A549 cells were reverse transfected with control non-targeting siRNAs (NT) or pooled siRNAs against ER stress sensors ATF-6A, ATF-6B, PERK, IRE-1alpha. Forty-three h post transfection cells were pre-incubated with DMSO or GCA for 5h (no addition=no pretreatment), inoculated with HAdV-C5-dE1_GFP and average nuclear GFP signal was analyzed 18 h pi. RU=relative units.

(B) IRE-1 knockdown by siPool-RNAs (siP) reduces HAdV-C5-dE1_GFP infection boost in GCA-treated A549 cells. siP Neg= non-targeting control siPool-RNAs. Intracellular IRE-1 levels were determined by Western blotting using β-tubulin as a loading control.

(C) GBF-1 inhibition by GCA induces ER stress and activates IRE-1 nuclease and splicing of XBP-1 mRNA. A549 cells were treated with GCA or the ER stress activator thapsigargin (Tg) for 5h, and IRE-1 activation was analyzed by PstI digestion of XBP1 cDNA amplicons. Spliced XBP-1 cDNA amplicon lacks a PstI site (1S), whereas the unspliced one retains the site and is cleaved into two fragments (2U and 3U) upon PstI digestion. Uppermost band * is a spliced/unspliced XBP-1 hybrid amplicon (24). XBP-1 splicing was inhibited by the IRE-1 nuclease inhibitor 4μ8C in GCA- and Tg-treated cells. GAPDH cDNA amplicons were used as a loading control.

(D) GCA-induced HAdV-C5-dE1_GFP infection boost in A549 cells requires IRE-1 endonuclease activation. Cells were pre-incubated with GCA or Tg for 5h with or without 4μ8C, inoculated with HAdV-C5-dE1_GFP and analyzed for GFP expression 18h pi.

(E) Reduced GCA infection boost in XBP-$1^{-/-}$ mouse embryo fibroblasts. XBP-$1^{+/+}$ or XBP-$1^{-/-}$ MEFs were pre-incubated with GCA, inoculated with HAdV-C5-dE1_GFP and analyzed for GFP expression 18 h pi.

(F) XBP-1 knockdown by siPool-RNAs (siP) reduces HAdV-C5-dE1_GFP infection boost in GCA-treated A549 cells. Cells were reverse transfected with siP-RNAs against XBP-1 or non-targeting control siP Neg, 72 h post transfection pre-incubated with GCA or DMSO for 5h, inoculated with HAdV-C5-dE1_GFP, and analyzed for GFP expression 18 h pi. Knockdown levels of the unspliced XBP-1 protein (XBP-1u) were controlled by Western blotting using β-tubulin as a loading control.

Figure 7: Inhibition of GBF-1 by GCA enhances spreading of virus infection via IRE-1 and XBP-1.

(A, B) Confluent A549 cells were pre-incubated with GCA for 5h and infected with replication competent HAdV-C2-dE3B_GFP (MOI 0.00016), and spreading of infection was analyzed by time-lapse fluorescence microscopy. (A) Spreading of infection is manifested by the typical comet phenotypes of infected GFP-positive cells. One of these comets is pointed out by an arrowhead. Arrowhead highlights one of many comets which increase in size as infection proceeds. (B) Quantification of the number of comets. The data is from two parallel experiments.

(C, D) A549 cells were reverse transfected with siPool negative control (siP Neg) RNAs or siPool RNAs against IRE-1 or XBP-1. Seventy-two h post transfection cells were pre-incubated with GCA or DMSO for 5h, inoculated with HAdV-C2-dE3B_GFP (MOI 0.008) and spreading of infection was analyzed by time-lapse fluorescence microscopy. (C) shows images from the 72 h pi recordings, and (D) shows the quantification of comets at the same time point. Data in (D) is from two parallel experiments.

Figure 8: Model for the UPR-induced HAdV infection boost by GCA.

ER stress can be induced by abnormal ER-associated lipids, redox potential, glycosylation, or protein flux through the secretory pathway, or by the depletion of calcium ions, for example by the Ca^{2+} ATPase inhibitor thapsigargin (29). Cells sense ER stress by three major pathways, the activating transcription factor 6 (ATF-6), the PKR-like ER kinase (PERK), and the inositol-requiring enzyme 1 (IRE-1) pathway. Here we show that the small compound Golgicide A (GCA), which blocks the guanine nucleotide exchange factor GBF-1 of Arf-GTPases implicated in ER-Golgi transport, induces the IRE-1/X-box binding protein 1 (XBP-1) branch of the UPR (depicted by green arrows). GCA and in some cases the knock-down of GBF-1 by siRNA enhances infection of cancer cells with both replicating and non-replicating human adenovirus (HAdV) of the C- and B-species. This requires the RNase activity of IRE-1, and leads to the splicing of the XBP-1 mRNA in the cytoplasm, yielding an mRNA, which encodes the active XBP-1 transcription factor (also dubbed XBP-1s). XBP-1 splicing can be blocked by the IRE-1 RNase inhibitor 4μ8C (13). XBP-1s may enhance the transcription of both host and viral genes, and thereby boost early and late viral gene expression, virus release from infected cells and viral spreading. Besides the XBP-1 branch, IRE-1 also signals through regulated IRE-1-dependent decay (RIDD) generating double-strand RNA (RNA*), and leading to activation of retinoic acid-inducible gene 1 (RIG-I), nuclear factor kappa-light-chain-enhancer of activated B cells (NFkB), and downstream cytokines and chemokines, which may boost HAdV infection (10, 17, 30, 39). A third output from IRE-1 signaling is the degradation of micro RNA 17 (miR17), an inhibitor of the apoptotic caspase 2 (68). If this pathway were triggered by GCA, it may enhance HAdV induced cell killing.

Annotations: Green arrows highlight the GCA pathway activating the IRE-1/XBP-1 branch of the UPR, and leading to HAdV infection boost, as shown in this work. Green dotted arrow denotes possible activations downstream of GCA-induced UPR. Blue dotted arrows relate to work previously published, and depict two signaling branches downstream of IRE-1 that could contribute to the enhancement of HAdV infection or cancer cell killing.

F1

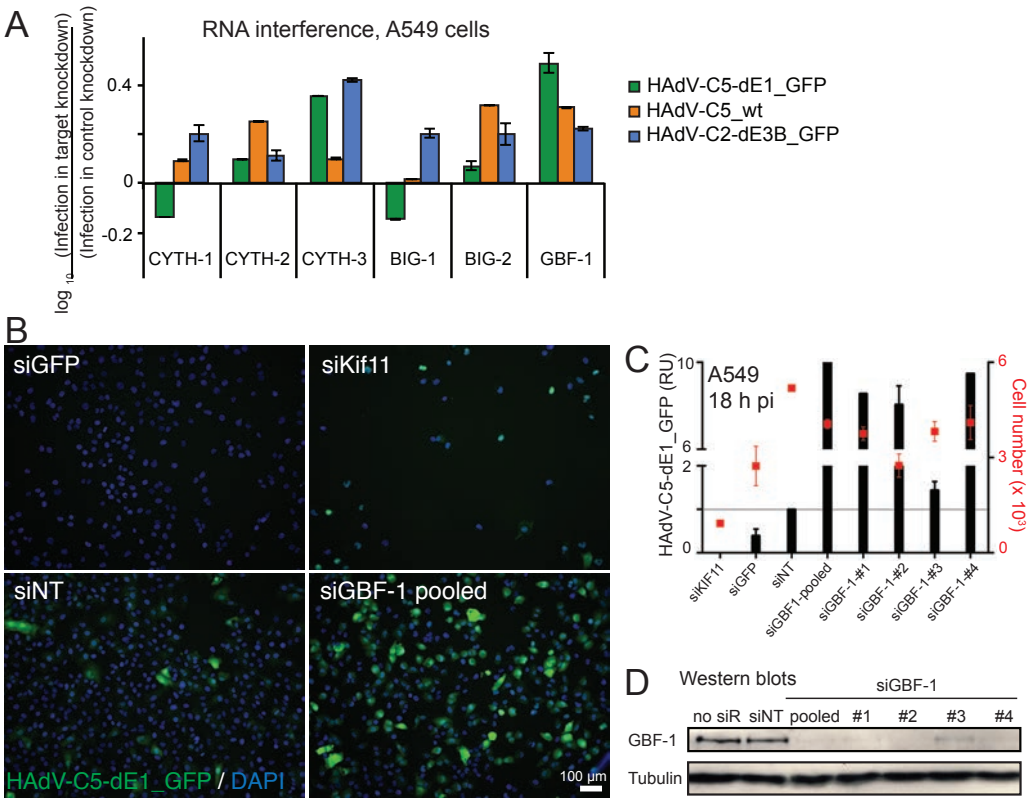
A
RNA interference, A549 cells
log10 (Infection in target knockdown) / (Infection in control knockdown)
0.4
0
-0.2
CYTH-1
CYTH-2
CYTH-3
BIG-1
BIG-2
GBF-1
HAdV-C5-dE1_GFP
HAdV-C5_wt
HAdV-C2-dE3B_GFP
B
siGFP
siKif11
siNT
siGBF-1 pooled
HAdV-C5-dE1_GFP / DAPI
100 µm
C
A549
18 h pi
HAdV-C5-dE1_GFP (RU)
Cell number (x 10³)
siKIF11
siGFP
siNT
siGBF1-pooled
siGBF-1#1
siGBF-1#2
siGBF-1#3
siGBF-1#4
D
Western blots
siGBF-1
no siR
siNT
pooled
#1
#2
#3
#4
GBF-1
Tubulin

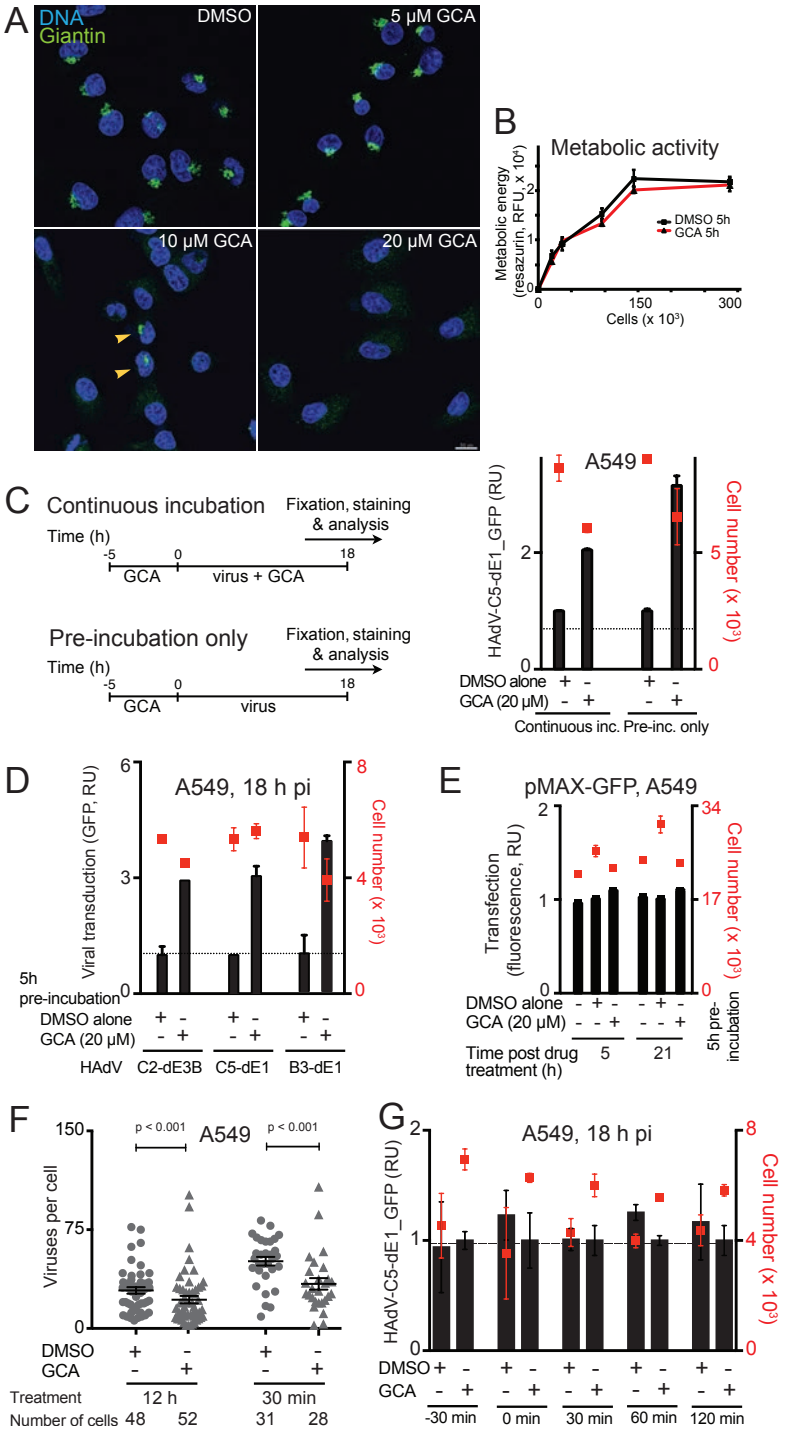
A
DNA
Giantin
DMSO
5 μM GCA
10 μM GCA
20 μM GCA
B
Metabolic activity
Metabolic energy (resazurin, RFU, x 10⁴)
DMSO 5h
GCA 5h
Cells (x 10³)
C
Continuous incubation
Fixation, staining & analysis
Time (h)
GCA
virus + GCA
Pre-incubation only
virus
A549
HAdV-C5-dE1_GFP (RU)
Cell number (x 10³)
DMSO alone
GCA (20 μM)
Continuous inc.
Pre-inc. only
D
A549, 18 h pi
Viral transduction (GFP, RU)
5h pre-incubation
HAdV
C2-dE3B
C5-dE1
B3-dE1
E
pMAX-GFP, A549
Transfection (fluorescence, RU)
Time post drug treatment (h)
5h pre-incubation
F
A549
p < 0.001
Viruses per cell
DMSO
GCA
Treatment
12 h
30 min
Number of cells
48
52
31
28
G
A549, 18 h pi
-30 min
0 min
30 min
60 min
120 min

F3

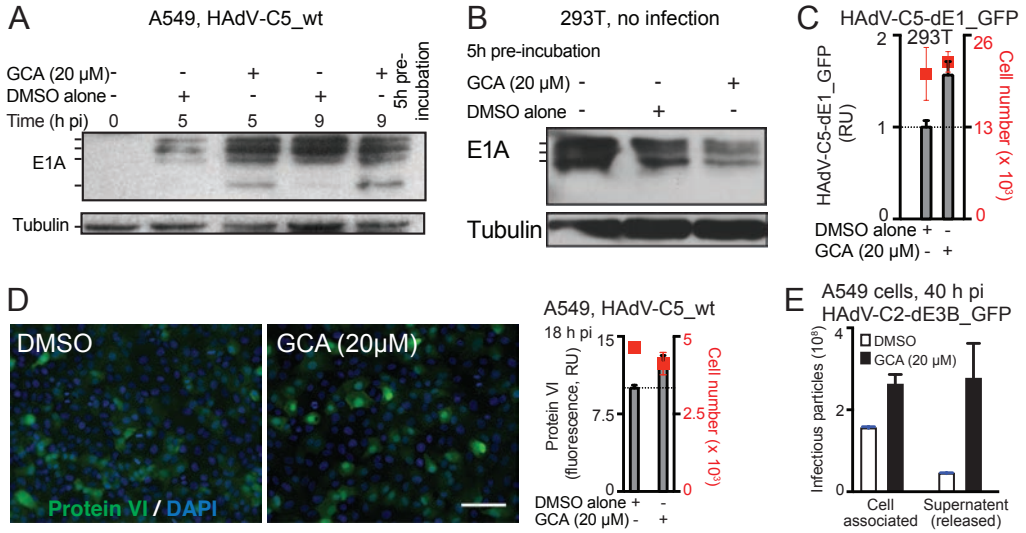
A
A549, HAdV-C5_wt
GCA (20 µM)
DMSO alone
Time (h pi)
5h pre-incubation
E1A
Tubulin
B
293T, no infection
5h pre-incubation
GCA (20 µM)
DMSO alone
E1A
Tubulin
C
HAdV-C5-dE1_GFP
293T
HAdV-C5-dE1_GFP (RU)
Cell number (x 10³)
DMSO alone
GCA (20 µM)
D
DMSO
GCA (20µM)
Protein VI / DAPI
A549, HAdV-C5_wt
18 h pi
Protein VI (fluorescence, RU)
Cell number (x 10³)
DMSO alone
GCA (20 µM)
E
A549 cells, 40 h pi
HAdV-C2-dE3B_GFP
Infectious particles (10⁸)
DMSO
GCA (20 µM)
Cell associated
Supernatent (released)

F4

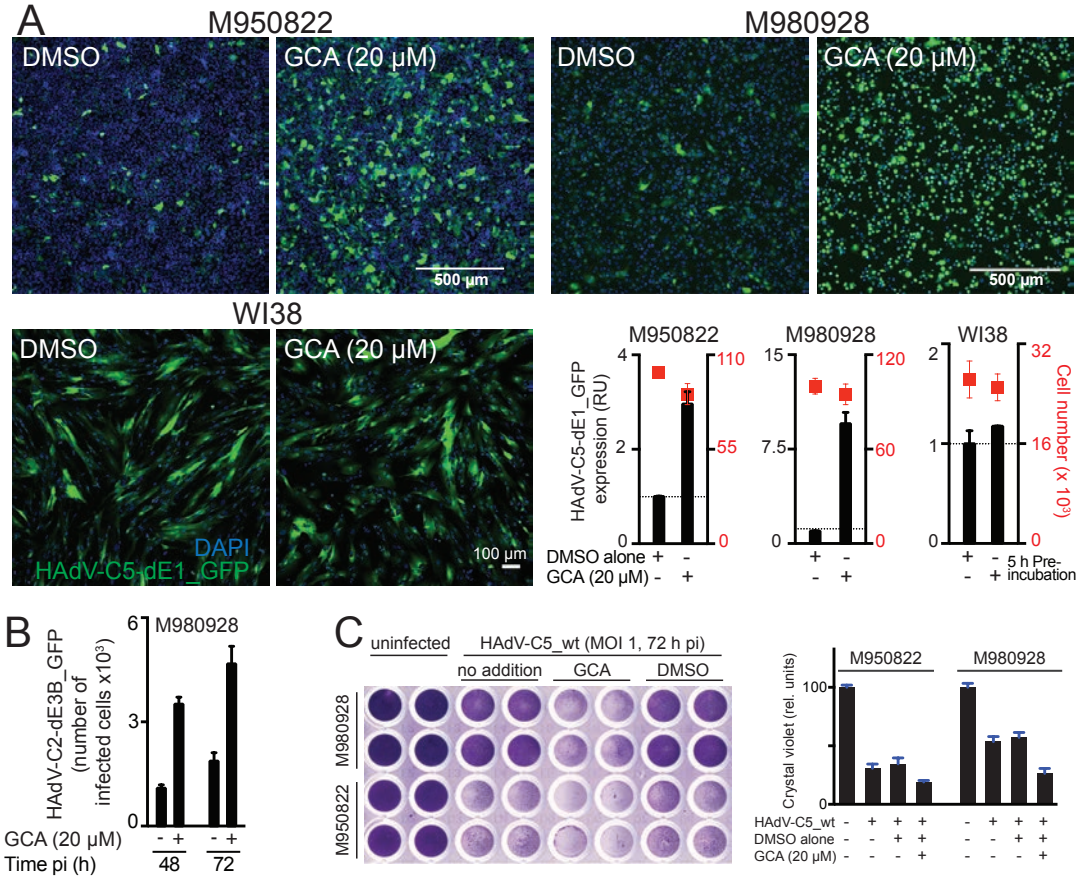
A
M950822
M980928
DMSO
GCA (20 µM)
500 µm
WI38
100 µm
DAPI
HAdV-C5-dE1_GFP
HAdV-C5-dE1_GFP expression (RU)
Cell number (x 10³)
DMSO alone
GCA (20 µM)
5 h Pre-incubation
B
HAdV-C2-dE3B_GFP (number of infected cells x10³)
GCA (20 µM)
Time pi (h)
48
72
C
uninfected
HAdV-C5_wt (MOI 1, 72 h pi)
no addition
GCA
DMSO
Crystal violet (rel. units)
HAdV-C5_wt

F5

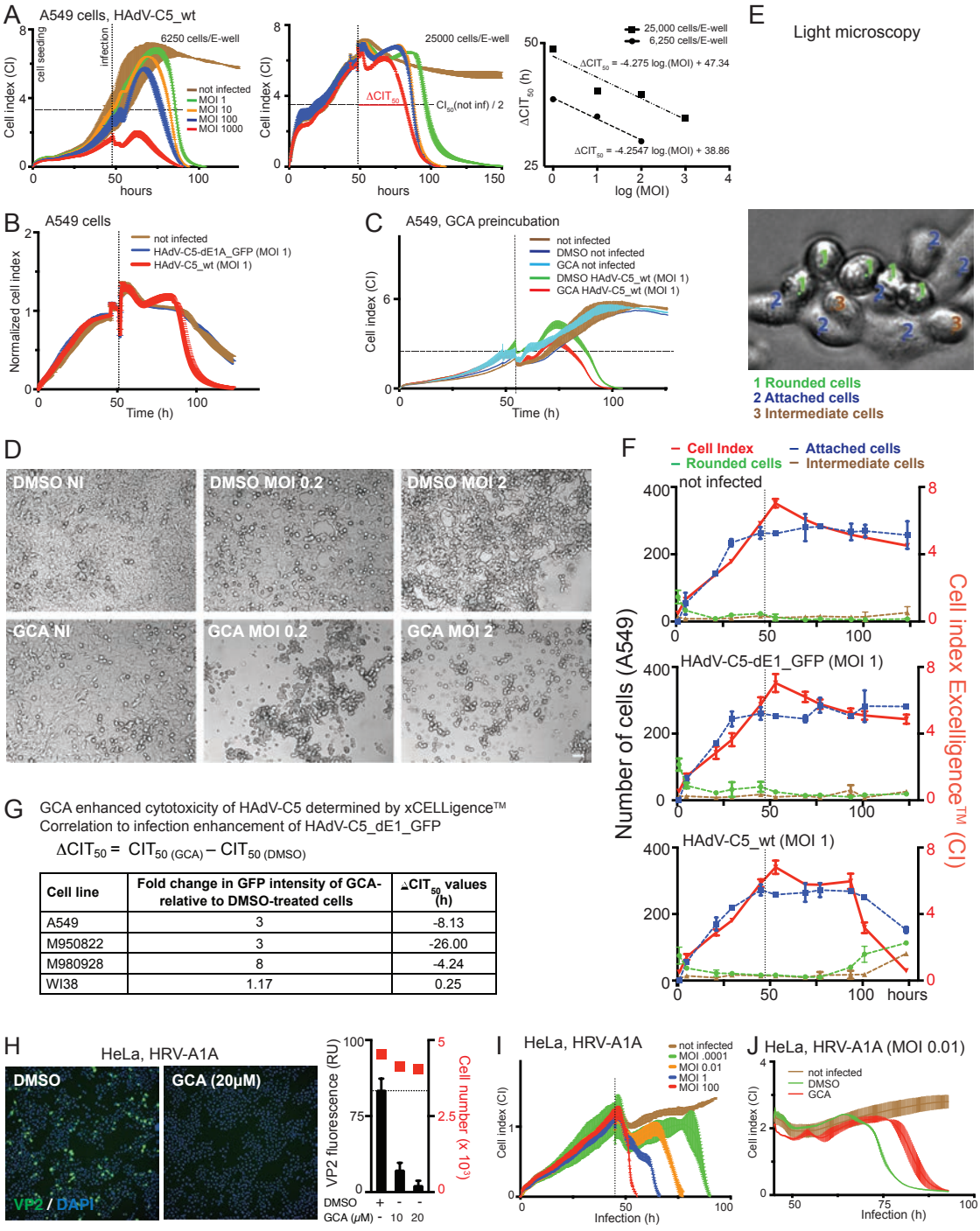

Cell line	Fold change in GFP intensity of GCA-relative to DMSO-treated cells	ΔCIT50 values (h)
A549	3	-8.13
M950822	3	-26.00
M980928	8	-4.24
WI38	1.17	0.25

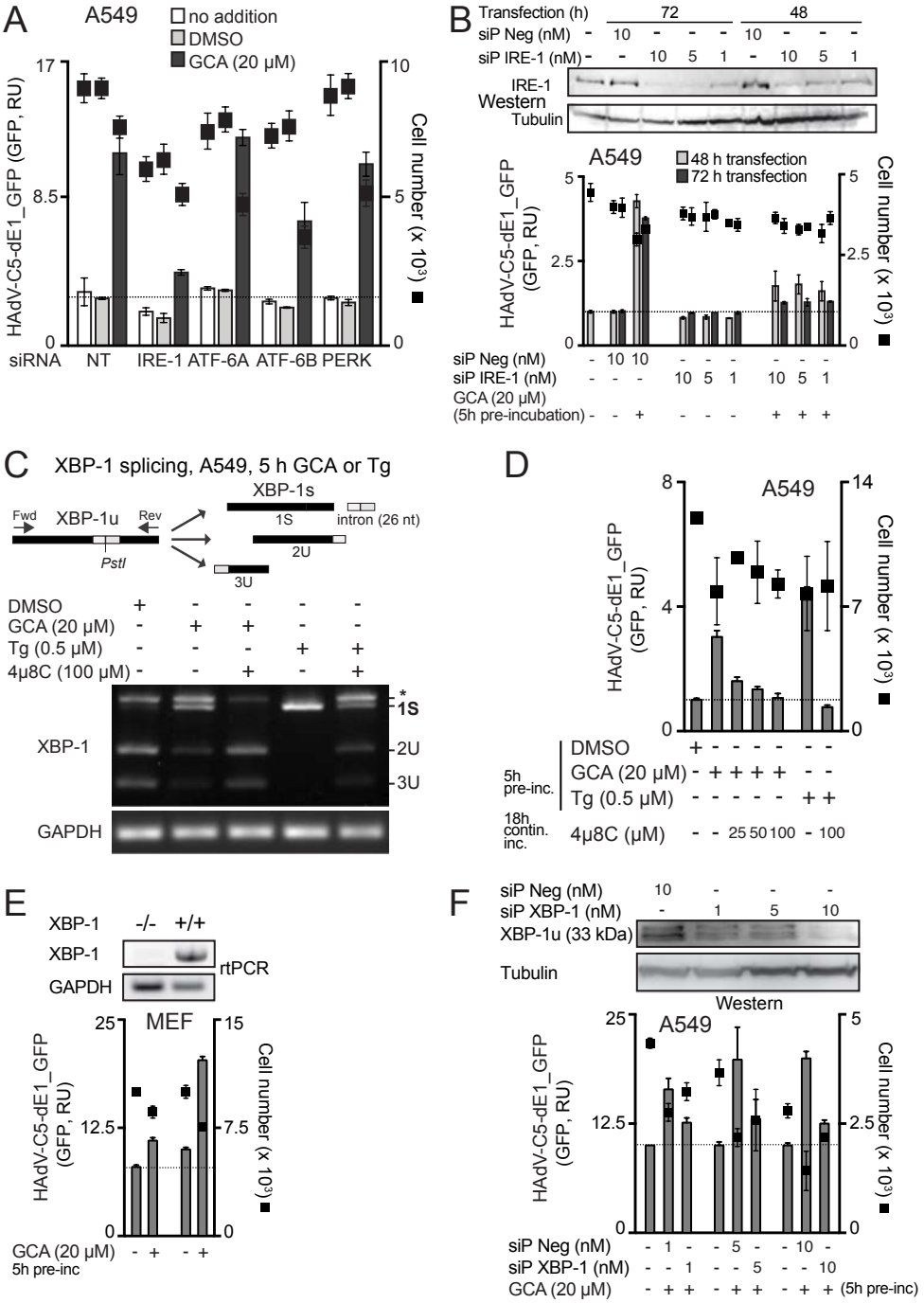
A
A549
no addition
DMSO
GCA (20 µM)
HAdV-C5-dE1_GFP (GFP, RU)
Cell number (x 10³)
siRNA NT IRE-1 ATF-6A ATF-6B PERK
B
Transfection (h)
siP Neg (nM)
siP IRE-1 (nM)
IRE-1
Western
Tubulin
A549
48 h transfection
72 h transfection
GCA (20 µM)
(5h pre-incubation)
C
XBP-1 splicing, A549, 5 h GCA or Tg
Fwd
XBP-1u
Rev
PstI
XBP-1s
1S
intron (26 nt)
2U
3U
DMSO
GCA (20 µM)
Tg (0.5 µM)
4µ8C (100 µM)
XBP-1
GAPDH
D
A549
HAdV-C5-dE1_GFP (GFP, RU)
Cell number (x 10³)
5h pre-inc.
18h contin. inc.
DMSO
GCA (20 µM)
Tg (0.5 µM)
4µ8C (µM)
E
XBP-1 -/- +/+
XBP-1
GAPDH
rtPCR
MEF
HAdV-C5-dE1_GFP (GFP, RU)
Cell number (x 10³)
GCA (20 µM)
5h pre-inc
F
siP Neg (nM)
siP XBP-1 (nM)
XBP-1u (33 kDa)
Tubulin
Western
A549
HAdV-C5-dE1_GFP (GFP, RU)
Cell number (x 10³)
GCA (20 µM)
(5h pre-inc)

F7

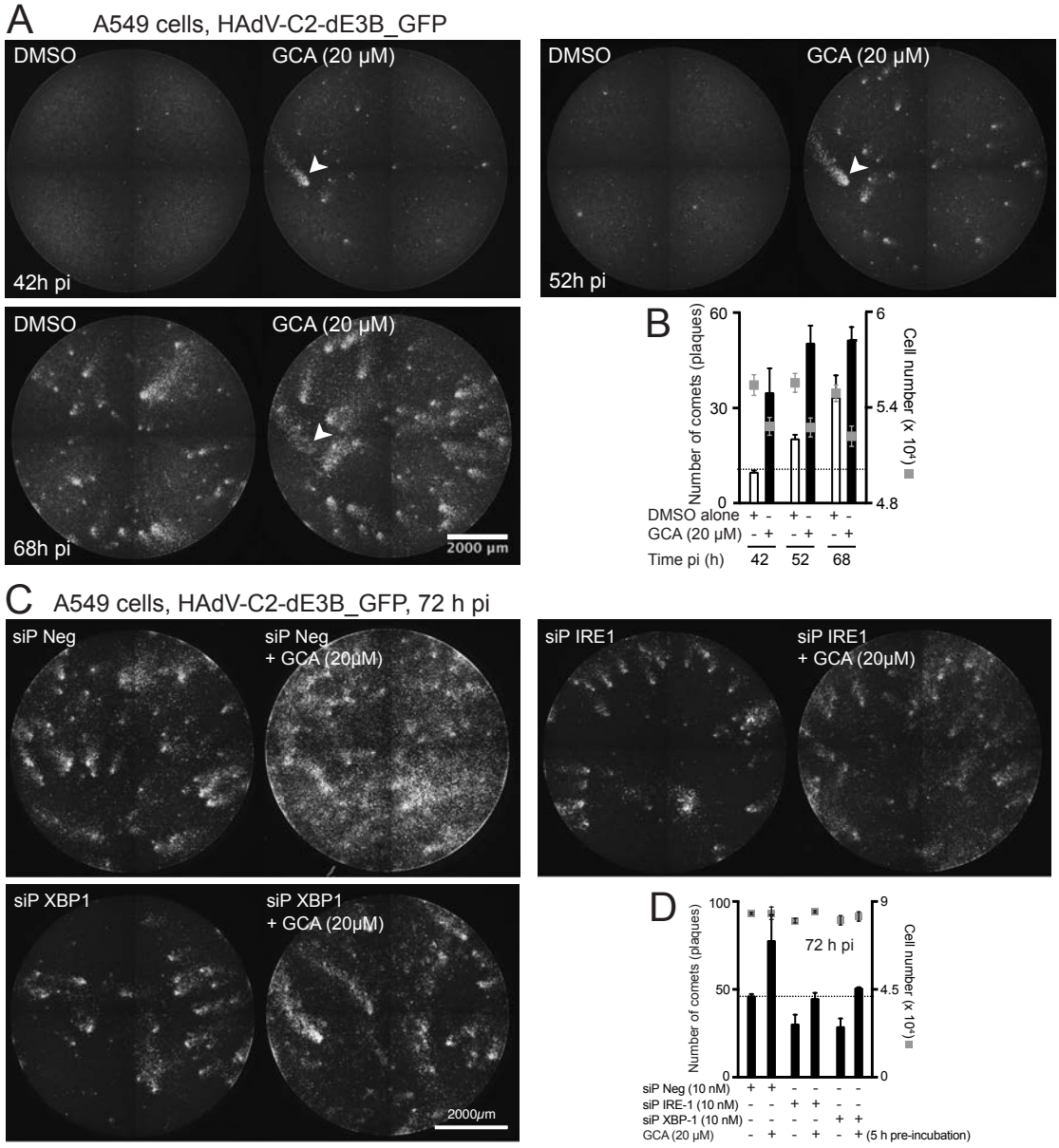
A
A549 cells, HAdV-C2-dE3B_GFP
DMSO
GCA (20 µM)
42h pi
DMSO
GCA (20 µM)
52h pi
DMSO
GCA (20 µM)
68h pi
2000 µm
B
Number of comets (plaques)
Cell number (x 10⁴)
60
30
0
6
5.4
4.8
DMSO alone + - + - + -
GCA (20 µM) - + - + - +
Time pi (h) 42 52 68
C
A549 cells, HAdV-C2-dE3B_GFP, 72 h pi
siP Neg
siP Neg
+ GCA (20µM)
siP IRE1
siP IRE1
+ GCA (20µM)
siP XBP1
siP XBP1
+ GCA (20µM)
2000µm
D
72 h pi
Number of comets (plaques)
Cell number (x 10⁴)
100
50
0
9
4.5
0
siP Neg (10 nM) + + - - - -
siP IRE-1 (10 nM) - - + + - -
siP XBP-1 (10 nM) - - - - + +
GCA (20 µM) - + - + - + (5 h pre-incubation)

F8

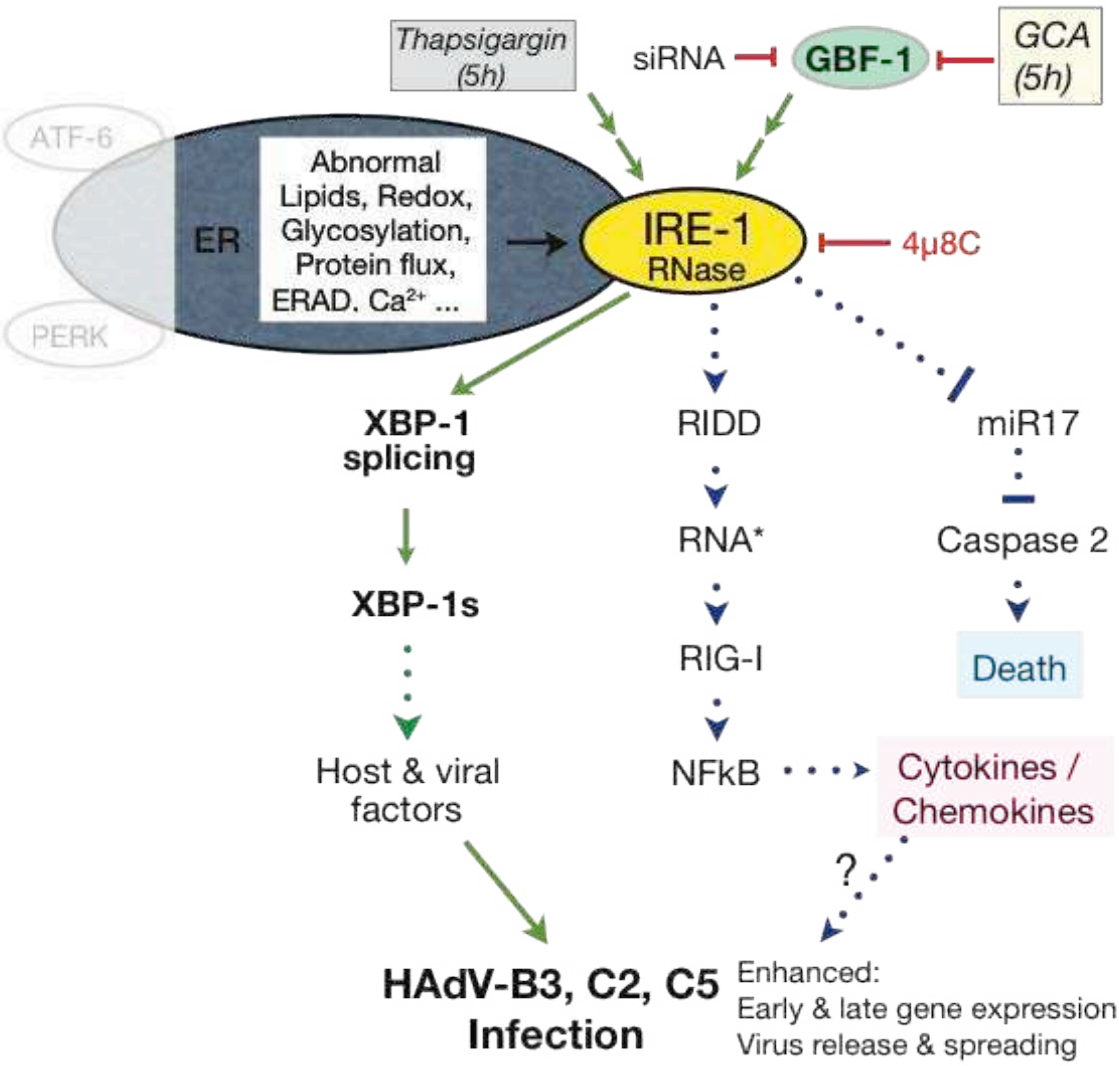
Thapsigargin (5h)
siRNA
GBF-1
GCA (5h)
ATF-6
ER
Abnormal Lipids, Redox, Glycosylation, Protein flux, ERAD, Ca2+ ...
IRE-1 RNase
4μ8C
PERK
XBP-1 splicing
RIDD
miR17
RNA*
Caspase 2
XBP-1s
RIG-I
Death
Host & viral factors
NFkB
Cytokines / Chemokines
?
HAdV-B3, C2, C5 Infection
Enhanced:
Early & late gene expression
Virus release & spreading